Structural and Conductive Characteristics of Fe/Co Nanotubes

**Shlimas DI[1,2],
Ibragimova MA[1],
Ibrayeva AD[1,2],
Kozlovskiy AL[1,2],
Zdorovets MV[1,2,3] and
Kadyrzhanov KK[2]**

1 Astana Branch of the Institute of Nuclear Physics, Astana, The Republic of Kazakhstan
2 LN Gumilyov Eurasian National University, Astana, The Republic of Kazakhstan
3 Ural Federal University, Ekaterinburg, The Russian Federation

Corresponding author: Anel Ibrayeva

✉ anelusha1991@mail.ru

Astana Branch of the Institute of Nuclear Physics, The Republic of Kazakhstan.

Tel: 77079067374

Abstract

In this paper we consider changing the conducting properties of Fe/Co nanotubes obtained by electrochemical deposition in the tracks of sample matrices based on PET. It is shown that the atomic metal ratio in the nanotubes obtained is shifted in favor of cobalt at increasing the potential difference. Using X-ray diffraction analysis it is revealed that the cobalt concentration growth in the crystal structure of the nanotubes leads to decreasing the interplanar space and increasing the conductivity value.

Keywords: Track membranes; Electrochemical deposition; Nanotubes; Nanotechnology

Introduction

Metallic nanostructures attract a great interest, as they have unusual optical, electronic, magnetic and chemical properties. There are various possibilities of their application in optoelectronic devices [1-3], as catalysts [4-8] in chemical reactions, as well as biosensors [9,10]. Template synthesis method is the most useful for metallic nanotubes and nanowires, when deposited structure has the same matrix shape. One method of such replica obtainment in the matrix pores by passing direct current through the electrolyte solution within the matrix, which also allows obtaining composite nanostructures. The main advantage of this method is the ability to control the rate of metal deposition in the pores by varying the current and the applied voltage, as well as the deposition time. Nanoscale objects with desired structure can be obtained adjusting these parameters [11-16].

In this paper, technique of creating Fe/Co nanotubes by template synthesis, characterization of their morphological properties, as well as the conducting properties dependence of the nanotube metals elemental composition. 12 microns thick polyethylene terephtalate (PET) membranes with a nominal diameter of about 110 nm obtained by ion-tracking technology are used as a template. Fe/Co deposition is carried out by the said electrochemical method at various deposition potentials.

Materials and Methods

Raw materials

Track membranes (TM) based on Hostaphan® type PET of «Mitsubishi Polyester Film» production company (Germany) were used for the template synthesis of Fe/Co nanotubes from the electrolyte solutions. Irradiation of 12 micron thick PET film was conducted at the DC-60 accelerator by krypton ions with 1.75 MeV/nucleon energy. Irradiation density was chosen to be $1.0E^{+09}$ pores/cm^2. After irradiation the film was exposed to a chemical bilateral etching in the 2M NaOH solution at 85 ± 0.1°C and then treated in neutralization solutions: 1.0% solution of acetic acid and deionized water. In this case pore diameter was 110 ± 5 nm.

Electrochemical deposition in PET TM channels

The nanotube synthesis in the template matrix tracks was performed at a voltage from 1.3 V, 1.5 V, 1.7 V and 2.0 V in potentiostatic mode. During the experiment voltage monitoring was carried out using the Agilent 34410A multimeter by chronoamperometry. Electrolyte solution used for the deposition of nanotubes was $CuSO_4 \times 7H_2O$ (110 g/l), $FeSO_4 \times 7H_2O$ (110 g/l), H_3BO_3 (25 g/l), $S_6N_8O_6$ (3 g/l). Control of the nanostructure growth

process was performed by chrono amperograms because their analysis allows studying the growth process dynamics.

Research of the Fe/Co nanotubes structure and properties

Study of the obtained nanotubes form and dimensions was carried out using a Hitachi TM3030 scanning electron microscope with Bruker XFlash MIN SVE microanalysis system at 15 kV accelerating voltage. X-ray diffraction researches were performed at D8 ADVANCE diffractometer using radiation of X-ray tube with Cu - anode and a graphite monochromator in the diffracted beam. Tube mode was 40 kV, 40 mA. Diffraction patterns were recorded in the angular range of 30-70°C 2θ with the step of 0.02° 2θ. Before structure research samples had been freed from the polymeric template by dissolving them in hot 9,0 M sodium hydroxide solution and subsequent treatment for 10 seconds in the ultrasonic bath to separate the polymer residues. HP 66312 A power supply and Agilent multimeter 34401 A were used to measure the current-voltage characteristics.

Results and Discussion

One feature of the electrochemical deposition is a possibility to control the properties of the synthesized nanostructures due to the predetermined pore geometry. Since the polymer matrices are insulators and do not conduct a current, before the electrochemical deposition process on the obtained templates 10 nm thick gold layer is deposited by magnetron sputtering under vacuum, what is a working electrode (cathode) during a deposition. In the works of Bond et al. has been showed that gold plated contacts in template [17,18] matrix pores in the form of rings on the pore walls are comparable in magnitude of current diffusion with monolithic discs, closing the pores completely. Thus, the electrode contacts in the form of rings on the pore walls obey Cottrell equation describing diffusion current 1:

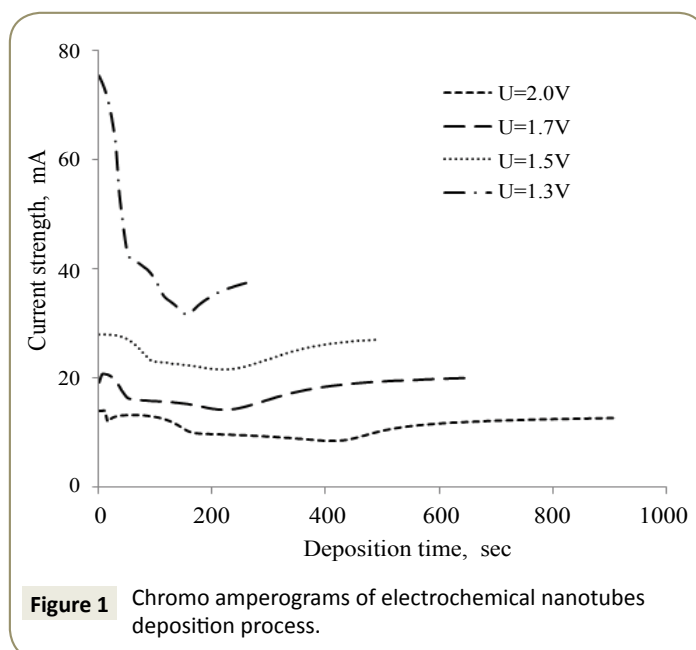$$i(t) = i_{d_{pore}} = \frac{4\pi FDc^b r^2}{4L + \pi r} \tag{1}$$

where n is a number of electrons participating in the reaction, F is the Faraday's number, r is a pore radius, D is a diffusion coefficient, c^b is a volume concentration of the solution, L is a membrane thickness. The rate of electrochemical processes, besides the mass transfer effect due to the diffusion controlled by the applied voltage magnitude, is also dependent on the effective area of the electrode surface. Since pores are randomly distributed in template matrices, the total equivalent area of the electrode surface is described by the formula 2.

$$S = 1 - \exp\left[\frac{4N\pi^3(D\pi)^{1/2}}{(4L + \pi r)} \frac{c^b}{c^b - c^m}\right] \tag{2}$$

where N is a pore density, c^m is the electrolyte solution concentration in pores. According to the Faraday's Law, the amount of deposited metal is directly proportional to the current or the current density. Thus, the following expression $i_{eq} = i_{pore}$ or $\pi r^2 j_{eq} = \pi r^2 j_{pore}$ can be written for the equivalent current value. During the electrochemical deposition process current changes can be expressed by expression 3.

$$i = j_{eq}S_{eq} = nF\left(\frac{D}{\pi r}\right)^{1/2} \cdot \left\{1 - \exp\left[\frac{4N\pi^3(Dt\pi)^{1/2}}{(4L + \pi r)} \frac{c^b}{c^b - c^m}\right]\right\} \tag{3}$$

Expression 3 qualitatively describes the experimental chrono amperograms of nanotubes synthesis process represented in **Figure 1.** The deposition time corresponding to the maximal length of the nanotubes (complete filling of the pore template) was determined based on the experimental chrono amperograms. The nanotube growth process was stopped at the beginning of the third stage to avoid a blockage or a «caps» formation on the surface of nanotubes designed to study the structural and magnetic characteristics. The research of the structural characteristics and morphology of the obtained nanostructures was performed using SEM. SEM - images of nanotubes are presented in **Figure 2.** Analyzing SEM–images of obtained nanostructures has shown that a height of nanotubes is equal to the template thickness of 12 microns and the diameter of 110 ± 5 nm. SEM analyzing the internal diameter of obtained nanotubes has not been conducted due to the insufficient resolution. The study of internal diameters in the PET template nanostructures was carried out by the manometric method to determine the gas permeability, based on measuring changes in gas pressure in the closed chamber at pressures in the range of 0.008 to 0.020 MPa with 0.004 MPa steps. **Figure 3** presents a graph demonstrating changes in the wall thickness from the volume deposition rate. The graph shows that that the wall thickness is reducing according to the law y=0.0148 × $^{-0,2411}$ with increasing the nanotube growth rate. Declining the thickness of the nanotube walls with rising deposition voltage can be justified on the basis of the following considerations. During electrochemical deposition the nanotubes growth is caused by two mechanisms the existing grains growth and the new grains generation, followed by the new layers formation. The 2nd growth mechanism becomes dominant with increasing deposition voltage, which leads to the growth of the volume rate of nanotubes growth and to quicker filling the pores with reducing wall thickness. The power dispersive analysis of the obtained nanostructures was carried out to determine the potential difference effect on the phase composition of the deposited nanotubes. **Figure 4** shows the EDX spectra of
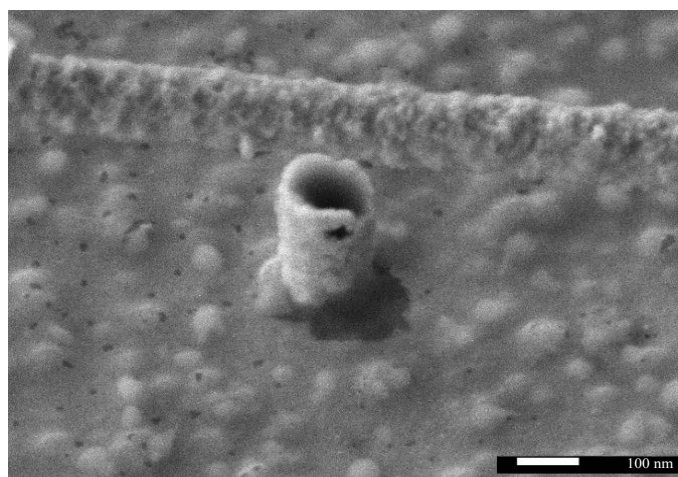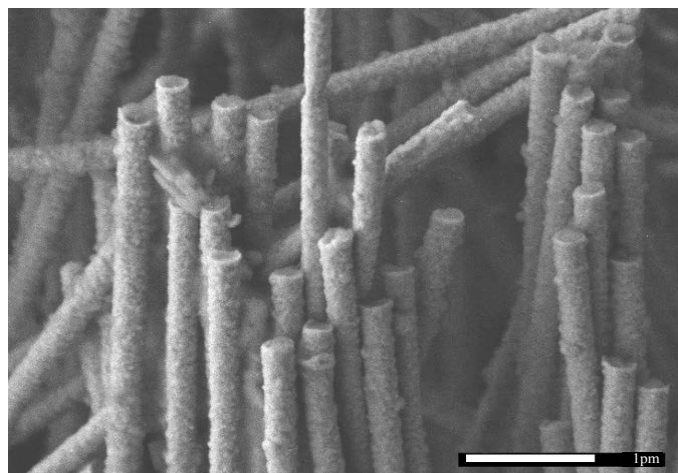

Figure 1 Chromo amperograms of electrochemical nanotubes deposition process.

difference (error in determining the composition was ~ 2%). During the synthesis, a growth of the applied potential in a cell becomes closer by a value to the recovery cobalt potential from the electrolyte solution prevailing over the iron reduction potential in the two-component electrolyte at the same concentration of salts by weight (50/50). X-ray diffraction study was conducted to determine the phase composition of Fe/Co nanotubes. As a result, it has been found that the investigated samples are single-phase with BCC structure and lattice parameter, which are
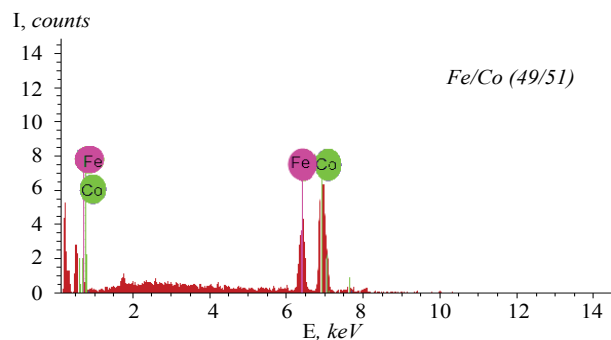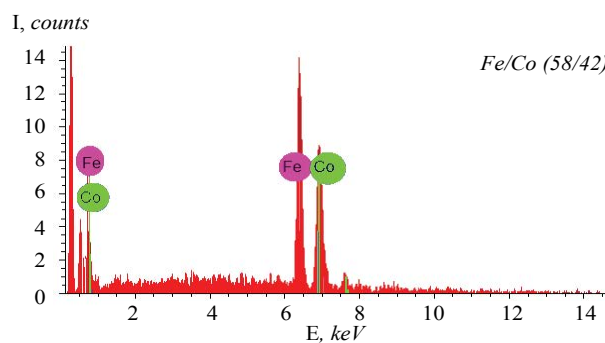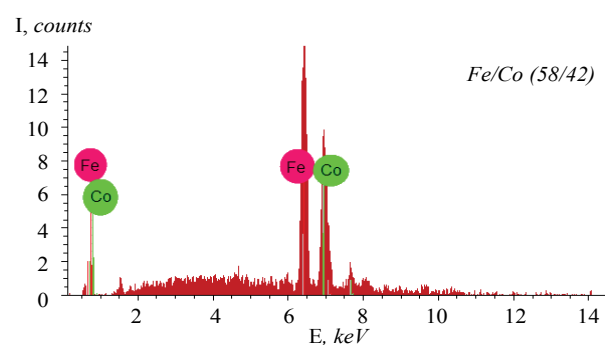

| **Figure 2** | Sem sample pictures of Fe/Co nanotubes obtained at 1.7 v potential difference a) -array, b) -tube sample. |

$$y = 0{,}0148x^{-0{,}2411}$$
$$R^2 = 0{,}9748$$
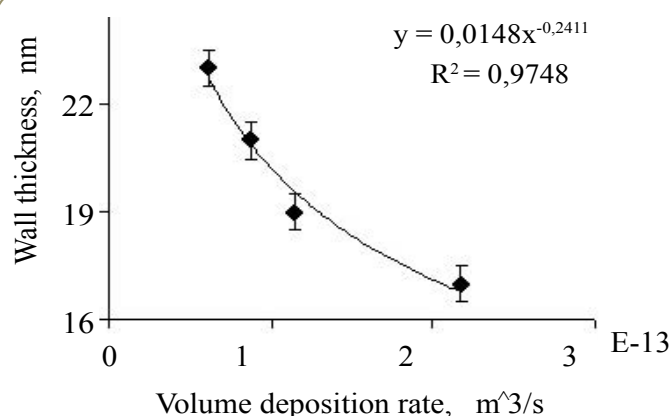
| **Figure 3** | Graph of wall thickness changes depending on volume deposition rate. |

the nanotubes deposited at different voltages. The gold peaks presence in the spectra corresponds to the substrate deposited on the PET membrane to make a conductive layer. Based on the results we can conclude that: atomic ratio of metal in produced nanotubes is shifted in favor of cobalt with increasing the potential
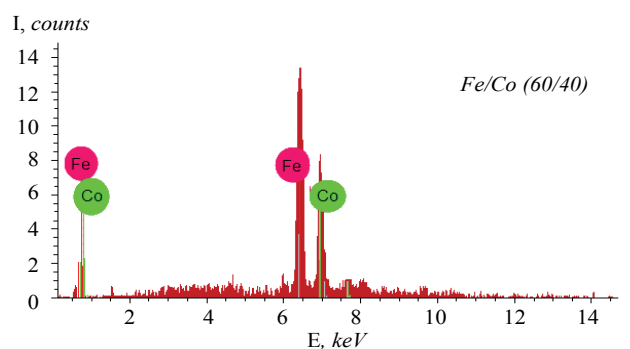

| **Figure 4** | EDX spectra of Fe/Co nanotubes a) -1.3 v b) -1.5 v c) -1.7 v and d) -2 v. |

different from the reference value. Since the obtained value has become slightly more than the standard sample value that the observed phase can be assumed to be a solid solution of cobalt substitution for iron. According to the literature BCC structure is typical for Fe/Co nanotube arrays containing Co more than 90% [19] and the films containing cobalt >85% [20]. The smaller width at the half height (the FWHM) of the main diffraction line (110) on the X-ray (0.722° for $Fe_{60}Co_{40}$, 0.706 for $Fe_{58}Co_{42}$, 0.702 for $Fe_{55}Co_{45}$ and 0.695 for $Fe_{49}Co_{51}$) indicates increasing the crystallinity degree with decreasing atomic iron content in nanotubes. Unit cell parameters were determined as a result of processing X-ray pictures. Graph of the unit cell parameter depending on the cobalt concentration in the nanotubes is shown in **Figure 5.** Approximating the obtained dependence it has been found that the unit cell parameter decreases with increasing cobalt concentration almost linearly with the coefficient Å. Obviously, the decrease of the unit cell parameter is associated with the difference of atomic radii r of Fe and Co, which are: equal to r (Fe)=1.227 Å, r (Co)=1.191 Å. According to the Scherrer equation the average crystallite size is (4):

$$\tau = \frac{k\lambda}{\beta \cos\theta},\qquad(4)$$

where k=0.9 is the dimensionless ratio of the particles form (the Scherrer's constant), λ=1.54 Å is a X-ray wavelength, β is a reflex half-width at half-maximum (FWHM) and θ-the angle of diffraction (Bragg angle). **Figure 6** demonstrates a graph of the average crystallite size depending on the cobalt concentration in the nanotubes. It can be seen from the resulting graph that increasing the Co concentration in the crystal structure of nanotubes leads to decreasing the average crystallite size. Current-voltage characteristics were recorded from the nanotubes array with area of 1.5 cm². **Figure 7** shows plots of current-voltage characteristics of the researched nanotubes. The graphs show that dI/dU angle grows with CO concentration increase in the obtained nanotubes. The nanotube array specific conductivity is calculated using the formula (5):

$$\sigma = \frac{dI}{dU}\frac{l}{A}\qquad(5)$$

where l is a length of nanotubes, A is an area, dI/dU is a tangent of I-U tilt angle. The result of the conductivity changes are shown in **Figure 7.** It is demonstrated that the specific conductivity increases with the potential difference growth at the Fe/Co nanotubes deposition, which leads to rising Co concentrations.

Conclusion

In this paper we consider the influence of deposition conditions on the phase composition, crystal structure and conducting properties of Fe/Co nanotubes, obtained by electrochemical deposition. It has been found that the atomic ratio of metals in the obtained nanotubes increases in favor of cobalt with the potential difference growth at the Fe/Co nanotubes deposition. X-ray analysis has showed that the tested samples are single phase with a BCC structure with a lattice parameter which is different from the reference value. Decreasing FWHM value of the main diffraction line (110) on X-ray pictures indicates the crystallinity growth with increasing the atomic cobalt content in nanotubes, while the amount of conductivity is also rising with cobalt concentration growth in the nanotube structure. Thus, the ordered arrays of magnetic nanotubes can be obtained
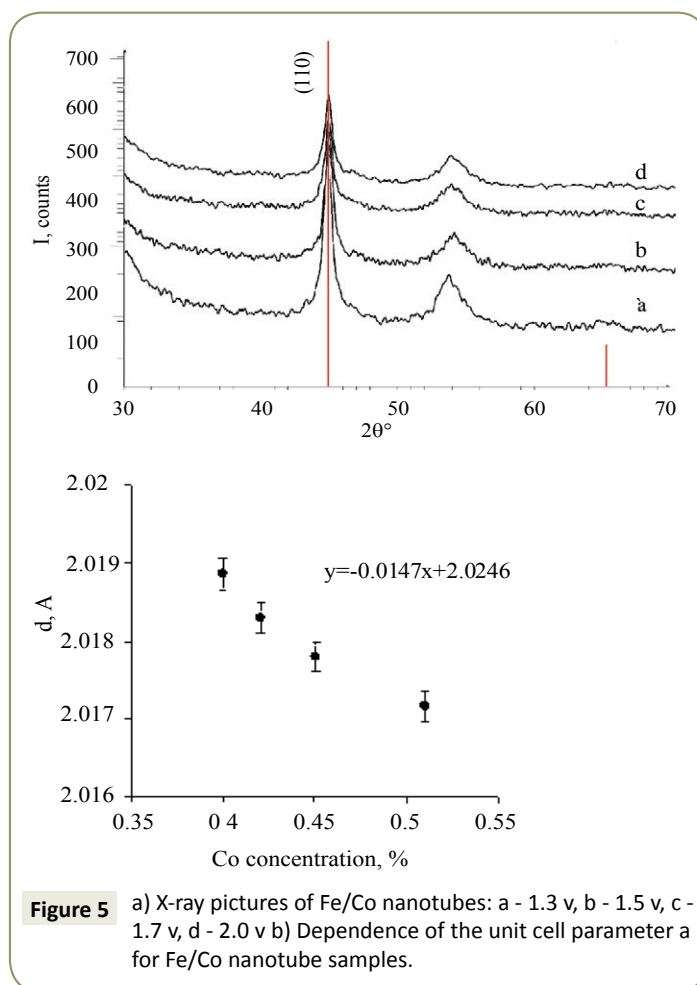

Figure 5   a) X-ray pictures of Fe/Co nanotubes: a - 1.3 v, b - 1.5 v, c - 1.7 v, d - 2.0 v b) Dependence of the unit cell parameter a for Fe/Co nanotube samples.
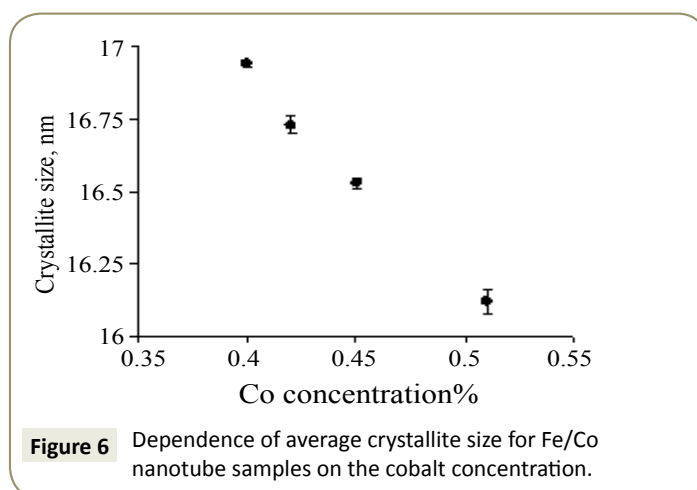

Figure 6   Dependence of average crystallite size for Fe/Co nanotube samples on the cobalt concentration.

controlling the phase composition and conductive properties of the nanotubes by changing the potential difference during the electrochemical deposition, so they can be used to make magnetic carriers based on nanostructures.

Funding

Figure 7 a) CVC graphs of Fe/Co nanotubes b) Graph of the conductivity change depending on the potential difference of Fe/Co nanotubes.
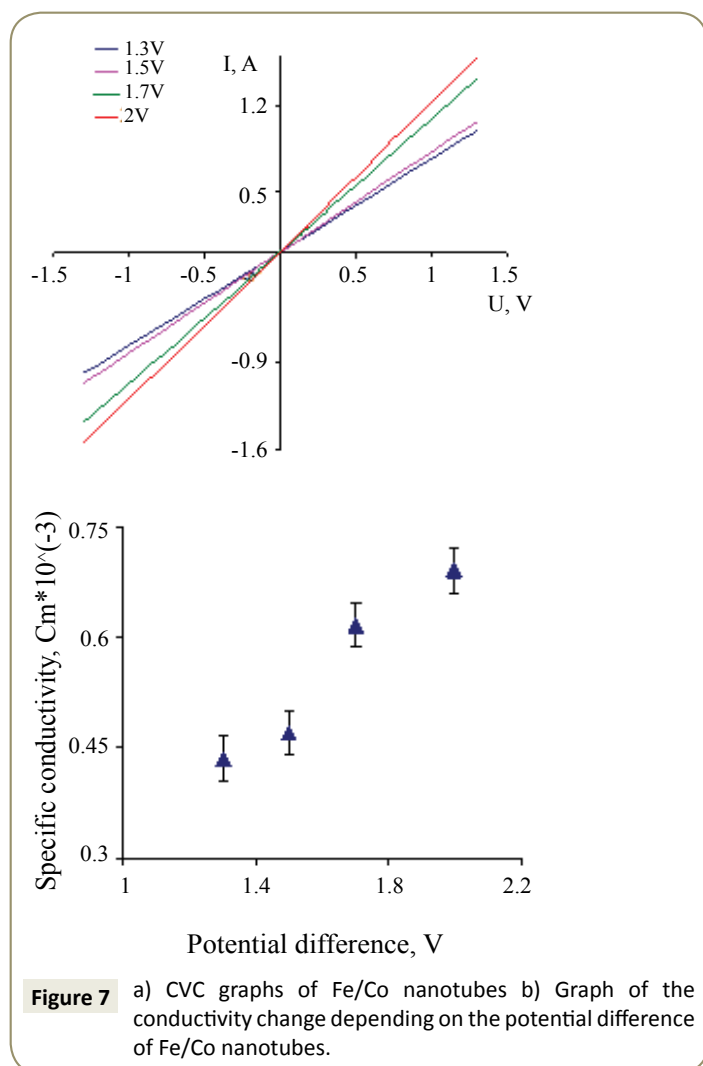
References

1   Hulteen JC, Martin CRJ (1997) A general template-based method for the preparation of nanomaterials. Mater Chem 7: 1075-1087.

2   Chakarvarti SK, Vetter J (1998) Template synthesis - a membrane based technology for generation of nano-/micro materials: a review. Radiation Measurements 29: 149-159.

3   Piraux L, Dubous S, Demoustier CS (1997) Nuclear Instr Meth Phys Res 131: 357.

4   Fink D, Petrov AV, Rao V (2003) Production parameters for the formation of metallic nanotubules in etched tracks. Rad Meas 36: 751-755.

5   Gopalan VE, Malini KA, Santhosh KG (2010) Template-Assisted Synthesis and Characterization of Passivated Nickel Nanoparticles. Nanoscale Res Lett 5: 889-897.

6   Stortini AM, Moretto LM, Mardegan A (2015) Sensors and Actuators 207: 186-192.

7   Gehlawat D, Chauhan RP (2014) Swift heavy ions induced variation in the electronic transport through Cu nanowires. Materials Chemistry and Physics 145: 60-67.

8   Chauhan RP (2014) Ion beam fluence induced variation in optical band-gap of ZnO nanowires. Journal of Experimental Nanoscience 9: 871-876.

9   Amandeep K, Chauhan RPJ (2013) Modifications induced by silicon and nickel ion beams in the electrical conductivity of zinc nanowires. Mater Sci Mater Electron 24: 4302-4310.

10 Gehlawat D, Chauhan RP (2014) Study of electronic transport in gamma ray exposed nanowires. Materials Research Bulletin 49: 454-461.

11 Duan J (2009) Nuclear Instruments and Methods in Physics Research 267: 2567-2570.

12 Nasirpouri F (2007) GMR in multilayered nanowires electrodeposited in track-etched polyester and polycarbonate membranes. Journal of Magnetism and Magnetic Materials 308: 35-39.

13 Azarian A (2009) Field emission of Co nanowires in polycarbonate template. Thin Solid Films 517: 1736-1739.

14 Baranova LA (2010) Nickel field-emission microcathode: Art of fabrication, properties, and applications. Nuclear Instruments and Methods in Physics Research 268: 1686-1688.

15 Adam (2008) Appl Phys Lett 92: 012516.

16 Sanchez BJ (2007) Magneto electrolysis of Co nanowire arrays grown in a track-etched polycarbonate membrane. Journal of Magnetism and Magnetic Materials. 312: 99-106.

17 Bond AM, Luscombe D, Oldham KB, Zoski CGJ (1988) Theory of electrochemical processes at an inlaid disc microelectrode under steady-state conditions. Electro anal Chem 245: 71.

18 Bond AM, Fleischmann M, Robinson JJ (1984) Electrochemistry in organic solvents without supporting electrolyte using platinum microelectrodes. Electro anal Chem 168: 299.

19 Chen Z, Zhan Q, Xue D, Li F, Zhou XJ (2002) Mossbauer study of Fe-Co nanowires. Phys Condens Matter 14: 613-620.

20 Hunter D, Osborn W, Wang K, Kazantseva N (2011) N Giant magnetostriction in annealed Co1−xFex thin-films. Nat Commun 2: 518.